Transport Measurements of Surface Electrons in 200 nm Deep Helium-Filled Microchannels Above Amorphous Metallic Electrodes

A. T. Asfaw,[1,*] E. I. Kleinbaum,[1] M. D. Henry,[2] E. A. Shaner,[2] and S. A. Lyon[1]

[1] *Department of Electrical Engineering, Princeton University, Princeton, New Jersey 08544, USA*
[2] *Sandia National Laboratories, Albuquerque, New Mexico, USA*

(Dated: March 1, 2022)

We report transport measurements of electrons on helium in a microchannel device where the channels are 200 nm deep and 3 μm wide. The channels are fabricated above amorphous metallic $Ta_{40}W_{40}Si_{20}$, which has surface roughness below 1 nm and minimal variations in work function across the surface due to the absence of polycrystalline grains. We are able to set the electron density in the channels using a ground plane. We estimate a mobility of 300 $cm^2/V{\cdot}s$ and electron densities as high as $2.56{\times}10^9$ cm^{-2}. We demonstrate control of the transport using a barrier which enables pinchoff at a central microchannel connecting two reservoirs. The conductance through the central microchannel is measured to be 10 nS for an electron density of $1.58{\times}10^9$ cm^{-2}. Our work extends transport measurements of surface electrons to thin helium films in microchannel devices above metallic substrates.

For nearly five decades, the system of electrons floating on the surface of bulk helium has provided a physical platform for studying a wide variety of phenomena[1, 2]. The phase diagram of this system can be further enriched at high electron densities where polaronic states, degenerate electron fluids and superconductivity are predicted to exist [3, 4]. This region of the phase diagram is difficult to achieve due to two fundamental barriers. First, bulk helium exhibits a hydrodynamic instability caused by the pressure of the electrons, which limits the maximum achievable electron density above the helium[5, 6]. Second, because of the strong electron-electron interaction at high densities, the Wigner crystal dominates the phase diagram for temperatures below 1 K[7].

These issues can be mitigated by using thin helium films on a dielectric substrate [4, 5, 8]. The van der Waals interaction between the helium and the substrate stiffens the film, pushing the hydrodynamic instability to higher electron densities. Further, the presence of the dielectric introduces an image charge which screens the Coulomb interaction and reduces the area of the Wigner crystal in the phase diagram. With the use of substrates that have large dielectric constants, the shielding can be enhanced. A metallic substrate would provide the highest density electron fluid.

A large body of experimental work has pursued these ends. While there is a significant body of work which has examined transport of electrons above insulating substrates, there have been fewer studies of electron transport on metallic substrates[5, 9]. The disparity between these two seemingly similar systems arises from the presence of disorder in metallic substrates, which can easily suppress electron transport above the metal and prevent basic transport measurements[10].

In this work, we fabricate and measure transport of electrons on a thin film of helium above an amorphous metallic substrate in a microchannel device. In contrast with typical polycrystalline metals, amorphous metals are defined by the lack of translational order on atomic length scales [11]. As a consequence, the surfaces of thin-film amorphous metals are exceptionally smooth and exhibit homogeneous work function over large areas, making them ideally suited for fabrication of electrodes for electrons on helium.

The amorphous metal used in this work is RF-sputtered $Ta_{40}W_{40}Si_{20}$ (hereafter TaWSi)[11–13]. Fig. 1a shows the topography of a 200 nm thick layer of TaWSi measured using atomic force microscopy in a 5 μm $\times$ 5 μm window, with a slice along the indicated line in the middle of the scan shown in Fig. 1b. The RMS roughness is measured to be less than 5 $\mathring{A}$, confirming the smoothness of the surface of the amorphous metal. In addition to these features, we have found that TaWSi is a superconductor with a critical temperature near 2 K. While this property of the metal has no noticeable effect on our measurements, it provides a method of integrating superconducting electronics[14].

An optical micrograph of the device is shown in Fig. 1c. Electrons are confined to two sets of 3 μm microchannels connected by a single central microchannel, similar to the device used by Rees *et al.* [15]. The microchannels are filled by the capillary action of superfluid helium, which determines the depth of helium in the channels. The channels are defined in a 170 nm layer of TaWSi, referred to as the ground plane. Below the ground plane is a 33 nm layer of insulating Al_2O_3 yielding 200 nm deep channels. Additional electrodes are defined in metallic layers beneath these channels. A 30 nm thick layer of chromium, referred to as the barrier, underlies the entire device. Above the barrier, the left and right reservoir electrodes are patterned in an additional 50 nm thick layer of TaWSi. Fig. 1d and e show cross-sections of the device along the microchannels above the reservoir electrodes and the central microchannel, respectively. The two reservoirs are separated by a 100 nm gap defined using electron-beam lithography.

* asfaw@princeton.edu

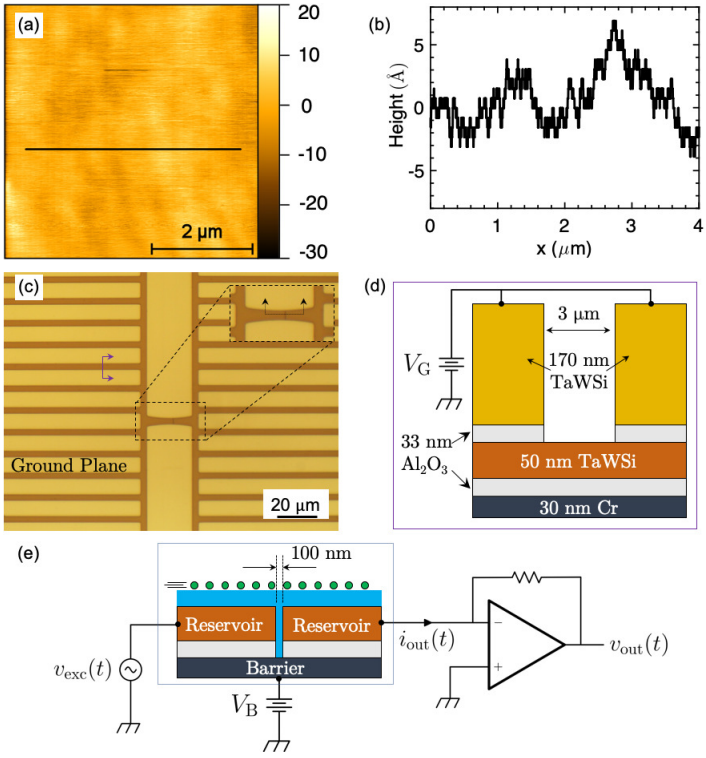

FIG. 1. (a) Topography of a 200 nm thick layer of RF-sputtered amorphous metallic $Ta_{40}W_{40}Si_{20}$ measured using atomic force microscopy in a 5 μm × 5 μm window. The colorbar is shown in units of Angstroms. The height profile along the indicated line in the middle of the scan is shown in (b). (c) Optical micrograph of the electrons on helium device. The channels are 200 nm deep and 3 μm wide. They are patterned on top of the left and right reservoir electrodes which are separated by a 100 nm gap as shown in the inset. (d) Cross-section of the device between the channels above the reservoir electrodes. (e) Cross-section of the device along the central microchannel. Figures (d) and (e) also show the electrical connections used throughout the measurements as described in the main text.

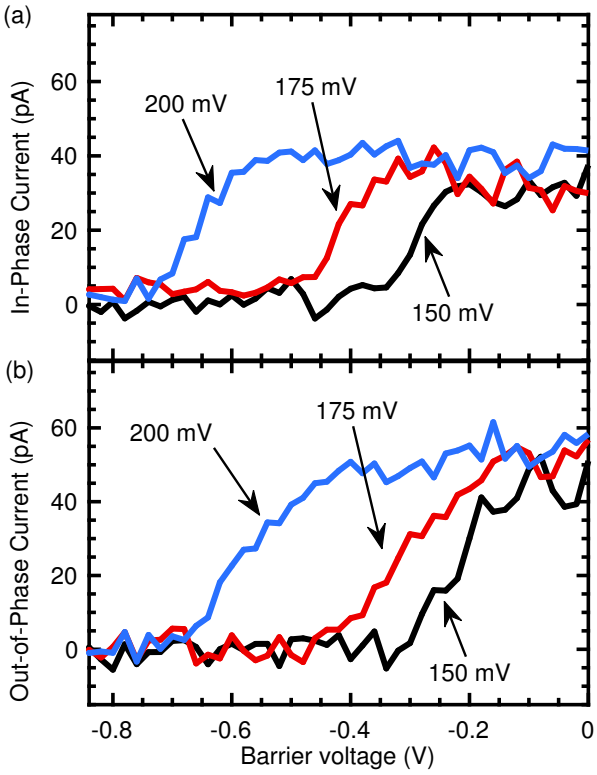

FIG. 2. Electron transport at three densities as a function of barrier voltage. Parts (a) and (b) show the in-phase and out-of-phase components of the signal measured from the right reservoir using lock-in detection. For electron densities of $\{1.58, 1.97 \text{ and } 2.56\}\times10^9$ cm^{-2} set by ground plane voltages $V_G = \{-150, -175 \text{ and } -200\}$ mV, the pinch-off barrier voltages are measured to be $V_B = \{-340, -480 \text{ and } -720\}$ mV, respectively.

The device is placed in a leak-tight copper cell 0.5 mm above the bulk helium level and cooled to a temperature of 1.7 K. Electrons are emitted onto the sample from a filament, with the ground plane voltage, V_G, set to -0.2 V and with all other electrodes at 0 V. Subsequently, an excitation voltage, $v_{exc}(t) = 10$ mV$_{RMS}$ is applied to the left reservoir electrode at a frequency of 260 Hz, and the resulting current, $i_{out(t)}$, is amplified by a current amplifier (Femto DLPCA-200) connected to the right reservoir electrode and measured using lock-in detection (Stanford Research Systems SR830).

We begin by measuring transport across the device while sweeping the barrier voltage, V_B more negative. Electrical transport through the central microchannel can be controlled by the barrier voltage akin to a field-effect transistor. At low barrier voltages, the central microchannel is open and allows current to flow between the two reservoirs. As the barrier in the central microchannel is increased by sweeping the barrier voltage more negative, the resistance of the central microchannel increases owing to the reduced density of electrons, as reflected by a reduction in the measured current. This behavior continues until the potential at the barrier exceeds the electron potential in the microchannels and the current is turned off completely. In Fig. 2a and b, we show the in-phase and out-of-phase current from the lock-in measurement for three ground plane voltages of $V_G = \{-150, -175, -200\}$ mV indicating pinch-off at barrier voltages $V_B = \{-340, -480, -720\}$ mV, respectively. These results can be interpreted by considering that more negative ground plane voltages increase the density of electrons in the microchannels, which in turn require larger barrier potentials at the central microchannel to cut off the transport.

In order to estimate the density of electrons in the microchannels corresponding to the above ground plane voltages, we open the barrier by setting it to 0 V and measure transport between the reservoirs as a function of the ground plane voltage, V_G. The results are shown in Fig. 3. For $V_G > -70$ mV, the channels above the left and right reservoir electrodes are depleted, resulting in

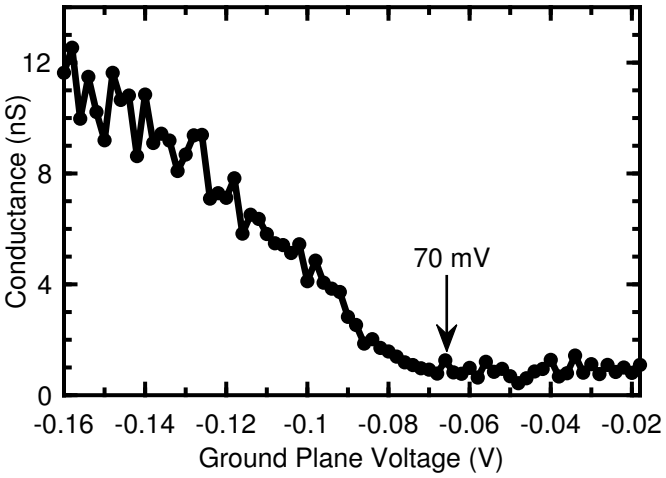

FIG. 3. Conductance of electron transport through the central microchannel. As the ground plane voltage exceeds $V_{\rm G} = -70$ mV, the conductance is observed to increase up to a value of 12 nS.

no measurable current through the central microchannel. On the other hand, for $V_G < -70$ mV, the conductance is seen to increase up to a saturation value of 12 nS. The voltage sweep shown in Fig. 3 was repeated multiple times, with no appreciable hysteresis, indicating that electrons are readily moved between the channels and the ground plane. In this case, the areal density, n, of electrons above the reservoir electrodes can be determined from the relation $n = \frac{\epsilon_0 \epsilon_{\rm He}}{d} \times (V_G + 70\ {\rm mV})/e$, where $\epsilon_{\rm He}$ is the dielectric constant of liquid Helium, ϵ_0 is the dielectric permittivity of free space, e is the electronic charge, and $d = 280$ nm is the thickness of the helium level above the reservoir electrodes estimated from the height of the sample above the bulk helium level in our cell. From this expression, we estimate the electron density above the microchannels to be $\{1.58, 1.97, 2.56\}\times 10^9$ cm^{-2} for ground plane voltages of $V_{\rm G} = \{-150, -175, -200\}$ mV, respectively. We note here that non-zero depletion voltage has been observed in other microchannel devices[15], and is likely due to a combination of work function differences between the different metallic layers as well as thermal offset voltages.

In order to estimate the mobility of the electron transport, we analyze the data for the ground plane voltage set to $V_{\rm G} = -150$ mV in detail. Assuming that the device can be modeled as a series RC circuit (R due to the central microchannel, and $2C$ due to coupling to the 2D electron gas in the microchannels above each reservoir electrode), we extract $1/R$ and C as a function of barrier voltage. The results of these calculations are shown in Fig. 4. We find that the total capacitance, C, remains nearly constant at a value of $\sim$4 pF once the barrier is opened, while the conductance increases up to a saturation value of $\sim$10 nS. The mobility can then be estimated from the expression $\rho/\Box = 1/ne\mu$ where $\Box \approx 8$ is the number of squares in the central microchannel, $\rho = (10\ {\rm nS})^{-1}$ is the 2D resistivity and $n = 1.58\times 10^9$ cm^{-2} is the density of electrons in the microchannels for $V_G = -150$ mV. From this expression, we estimate the mobility of transport in the channels to be 300 cm^2/V·s. In addition, from the total area of the microchannels above each reservoir of 0.54 mm^2, we estimate that the channels are half-filled at this density.

We remark here on the assumptions made in the estimate of the mobility. First, we have assumed that the resistance R of the transport comes entirely from the central microchannel. This assumption ignores the contribution of the ~ 900 μm long microchannels above the reservoirs to the resistance. Additionally, there is a 100 nm gap in the central microchannel that has been used to separate the left and right reservoir electrodes. As an electron moves between the reservoirs, it experiences a resistance due to the discontinuity seen by its image charge at the edges of the gap. Given that the gap width of 100 nm is comparable to the distance of the electron above the reservoir electrodes ($d \approx 280$ nm), it is likely that the edge contributes to the resistance of the transport. Our estimate of the mobility constitutes a lower bound as a result of these assumptions and further measurements are necessary to separately measure these contributions to the resistance.

The ability to perform measurements with shallow helium has two advantages – first, experiments with microchannel devices that have previously been used where the helium is of order 1 μm or thicker can now be extended to shallow helium levels where larger electron densities can be supported. The second benefit is that devices that are typically used in the study of solid-state quantum computation can be realized when gate electrodes can be patterned beneath thin helium films. For example, these gate electrodes can be used to electrostatically define quantum dots for individual electrons on helium, enabling the storage and manipulation of quantum information [16–19].

In conclusion, we have demonstrated transport of electrons on helium in a microchannel device where the channels are only 200 nm deep. The choice of amorphous $Ta_{40}W_{40}Si_{20}$ as the material for the fabrication of the channels has enabled transport at these depths where the surface roughness and work function variations across the surface are minimized. We have shown the ability to control the transport of electrons across reservoirs using a barrier as well as the ability to set the density of electrons using the ground plane. Future work will investigate shallow devices where higher electron densities can be supported. Additionally, the ability to work with shallow microchannels enables the design of devices where quantum-mechanical effects such as lateral tunneling between quantum dots can be observed.

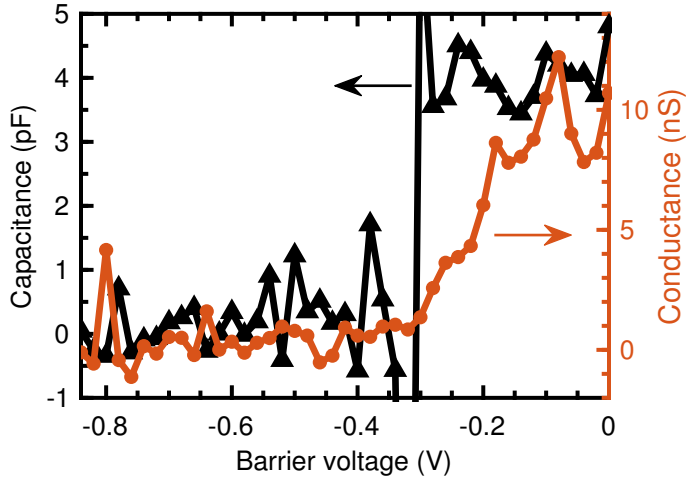

FIG. 4. Capacitance above reservoirs and conductance through the central microchannel for an electron density of 1.58×10^9 cm^{-2}. From the measured values, we estimate that the channels are half-filled above the reservoirs, and the mobility of electron transport is 300 cm^2/V·s.

ACKNOWLEDGMENTS

Devices were fabricated in the Princeton Institute for the Science and Technology of Materials Micro/Nano Fabrication Laboratory and the Princeton University Quantum Device Nanofabrication Laboratory. Work at Princeton was supported by the NSF, in part through Grant No. DMR-1506862, and in part through the Princeton MRSEC (Grant No. DMR-1420541). Sandia National Laboratories is a multimission laboratory managed and operated by National Technology & Engineering Solutions of Sandia, LLC, a wholly owned subsidiary of Honeywell International Inc., for the U.S. Department of Energy's National Nuclear Security Administration under contract DE-NA0003525. This paper describes objective technical results and analysis. Any subjective views or opinions that might be expressed in the paper do not necessarily represent the views of the U.S. Department of Energy or the United States Government.

[1] E. Y. Andrei, *Two-Dimensional Electron Systems on Helium and other Cryogenic Substrates* (Springer Netherlands, 1997).
[2] Y. Monarkha and K. Kono, *Two-Dimensional Coulomb Liquids and Solids* (Springer-Verlag, 2004).
[3] F. M. Peeters and P. M. Platzman, Phys. Rev. Lett. **50**, 2021 (1983).
[4] H. W. Jiang, M. A. Stan, and A. J. Dahm, Surface Science **196**, 1 (1988).
[5] H. Etz, W. Gombert, W. Idstein, and P. Leiderer, Phys. Rev. Lett. **53**, 2567 (1984).
[6] X. L. Hu and A. J. Dahm, Phys. Rev. B **42**, 2010 (1990).
[7] C. C. Grimes and G. Adams, Surface Science **98**, 1 (1980).
[8] G. Mistura, T. Gnzler, S. Neser, and P. Leiderer, Phys. Rev. B **56**, 8360 (1997).
[9] J. Angrik, A. Faustein, J. Klier, and P. Leiderer, Journal of Low Temperature Physics **137**, 335 (2004).
[10] J. Klier, I. Doicescu, P. Leiderer, and V. Shikin, J Low Temp Phys **150**, 212 (2008).
[11] J. M. McGlone, *Development of Amorphous Metal Thin Films for Thermal Inkjet Printing and Microelectronics*, Ph.D. thesis, Oregon State University (2017).
[12] J. M. McGlone, K. R. Olsen, W. F. Stickle, J. E. Abbott, R. A. Pugliese, G. S. Long, D. A. Keszler, and J. F. Wager, Journal of Alloys and Compounds **650**, 102 (2015).
[13] J. M. McGlone, K. R. Olsen, W. F. Stickle, J. E. Abbott, R. A. Pugliese, G. S. Long, D. A. Keszler, and J. F. Wager, MRS Communications **7**, 715 (2017).
[14] G. Yang, A. Fragner, G. Koolstra, L. Ocola, D. Czaplewski, R. Schoelkopf, and D. Schuster, Phys. Rev. X **6**, 011031 (2016).
[15] D. G. Rees, I. Kuroda, C. A. Marrache-Kikuchi, M. Hfer, P. Leiderer, and K. Kono, J Low Temp Phys **166**, 107 (2012).
[16] A. J. Dahm, Low Temperature Physics **29**, 489 (2003).
[17] M. I. Dykman, P. M. Platzman, and P. Seddighrad, Phys. Rev. B **67**, 155402 (2003).
[18] S. A. Lyon, Phys. Rev. A **74**, 052338 (2006).
[19] D. I. Schuster, A. Fragner, M. I. Dykman, S. A. Lyon, and R. J. Schoelkopf, Phys. Rev. Lett. **105**, 040503 (2010).